Low Shrinkage Metal Skeletons by Three Dimensional Printing

Emanuel Sachs[1], Samuel Allen[2], Costas Hadjiloucas[1], Jeannie Yoo[3], Michael Cima[2]

[1]Department of Mechanical Engineering, Massachusetts Institute of Technology, Cambridge, MA 02139
[2]Department of Materials Science and Engineering, Massachusetts Institute of Technology, Cambridge, MA 02139
[3]Imation Enterprises Corporation, 1 Imation Place, Oakdale, MN 55128-3414

Abstract

Three Dimensional Printing (3DP) is used to create metal parts by spreading a metal powder and printing a binder to define the geometry. In the currently used process a polymeric binder is used to define a green component. The polymer is burned out and the component lightly sintered to produce a skeleton. This sintering operation is causing 1.5 $\pm$ 0.2% shrinkage. The 3DP process can compensate for a given amount of predicted shrinkage by beginning with a larger part. However, the $\pm$ 0.2% uncertainty in the value of shrinkage translates directly to the loss of dimensional control of the parts. Therefore, there is a need to improve the dimensional control of metal parts produced by 3D Printing.

The current work investigates the possibility of decreasing the average shrinkage by eliminating the sintering step. The concept under investigation is an alternative method of forming the skeleton where the metal needed to create the necks between powder particles is provided through the binder - a salt solution. The metal is obtained from the salt by means of a heat treatment in a reducing atmosphere. It was found that strong metallic bonding can be obtained by melting the metal or the alloy derived from the salt solutions resulting, essentially, in brazing of the powder particles. Injection molding tools were fabricated by printing a copper nitrate solution into a dry mixture of 66μm molybdenum and 1μm silver powder. The metal skeletons were infiltrated with epoxies. The shrinkage caused by the brazing step on the 66μm Mo powder is approximately 0.15% which compares favorably with the 1.5% shrinkage obtained by the standard sinter-based method. It was hypothesized that the shrinkage of this new binding method is due to the capillary forces induced by the molten metal necks. The traction force due to molten metal necks was modeled analytically and the compressibility of the powder was measured. The shrinkage determined by the equilibrium of these two effects match observed shrinkages well. The model suggests certain approaches to the further reduction of shrinkage, including attaining a higher packing fraction of the powder-bed.

1 Introduction

1.1 Background

Three Dimensional Printing (3DP) is a process for the rapid fabrication of three dimensional parts directly from computer models [1-3]. A solid object is created by printing a sequence of two-dimensional layers. The creation of each layer involves the spreading of a thin layer of powdered material followed by the selective joining of powder in the layer by printing binder material. The powder bed is lowered at the completion of each layer by lowering the bottom of

the rectangular cylinder which contains the powder bed allowing for the next layer of powder to be spread. Unbound powder temporarily supports unconnected portions of the component, allowing overhangs, undercuts and internal volumes to be created. The unbound powder is removed upon process completion, leaving the finished part (green part).

An important application of the 3DP is in the direct printing of injection molding tools. This application has two focus areas : i) the rapid fabrication (within a day or two) of tooling for a few hundred prototype parts and ii) the fabrication of production tooling which has unique capabilities such as cooling lines which are conformal to the molding cavity [4]. Direct printing of tooling involves the following steps:

1) Geometry Definition: A polymeric binder is printed into stainless or tool steel powder to create the green part within the powder bed. The loose powder is removed, thereby revealing the green part.

2) Formation of Skeleton: The green part is placed in a ceramic powder (alumina and zirconia powders are usually used) in order to support the green part during sintering. The polymeric binder is burned out in a furnace (at 500 °C) and the part is lightly sintered (at 1200 °C). The ceramic powder does not sinter at this temperature and it can be removed after the heat treatment. At the end of this step the parts are strongly bonded due to the formation of necks between powder particles during sintering.

3) Infiltration: The part is infiltrated with a copper alloy in a second furnace operation, typically performed at 1200 °C. At the end of this step the part is fully dense.

4) Finishing: The tooling is finished to achieve desired surface finish and dimension as required.

1.2 Motivation

Tools made by the process described above have been successfully finished and used to injection mold parts in large quantity. A primary issue with this process is that the dimensional control is approximately ± 0.2% of the part dimension. The growth of the necks during the sintering step causes a shrinkage of the part which, in general, is not uniform and has a certain amount of error associated with it. As currently practiced, the magnitude of the shrinkage is 1.5% and the uncertainty is 0.2%. The 3DP process can compensate for a given amount of predicted shrinkage by beginning with a larger green part. However, the uncertainty in the value of shrinkage, translates directly to the loss of dimensional control of the parts. Therefore, there is a need to improve the dimensional control of metal parts produced by 3D Printing.

1.3 Approach to Eliminate Sintering

The current work investigates the possibility of decreasing the average shrinkage by eliminating the sintering step. The concept under investigation is an alternative method of forming the skeleton where the metal needed to create the necks between powder particles is

provided by adding it through the binder rather than relying on mass transport from the powder particles during the sintering operation.

Figure 1 illustrates one method that can be used to add metal through the printed binder: a salt solution is printed into the powder bed and then the entire (printed and un-printed) powder bed is fired at an appropriate temperature, resulting in the reduction of the salt to metal. After an appropriate heat treatment, the metal of the salt binds the printed powder.

The advantages of adding the metal by printing it in the binder include:

1) The elimination of the sintering step will most likely result in an average shrinkage significantly lower than the 1.5% of the current process. In addition, it is expected that the uncertainty (error) in shrinkage would be reduced commensurately.

2) The approach eliminates the need to burn out a polymer binder, a substantial convenience. Furthermore, some materials (i.e. titanium) are extremely sensitive to trace carbon left from the binder burn out.

3) The approach enables the firing of the printed parts in their original powder. Such a process eliminates the necessity to remove the green parts from their original powder bed and repack them in a ceramic powder. This is advantageous because the green parts are fragile and because the operation of packing the green parts in a ceramic powder-bed is difficult to do with reproducible results.

The following section discusses the formation of metallic skeletons bonded with necks derived from salt solutions and their application to the rapid fabrication of short run tooling. The shrinkage associated with the salt binding method and the experimental technique to measure it, is discussed in section 3. Section 4 presents a model for the shrinkage and provides direction for future work based on this model.

2 Metal Necks By Salt Reduction

2.1 Silver Carbonate on Mo Powder – Electrochemical Displacement Reaction

Silver carbonate (Ag_2CO_3) can be dissolved in an ammoniated solution of water. Droplets of a 0.3 molar solution of silver carbonate were placed onto 66μm Mo powder. The solvent consists of 87 v.o % H_2O and 13 v.o % ammonium hydroxide (ACS, 29.6% NH_3).

Upon contact with the Mo powder, silver is deposited on the powder by means of an electrochemical displacement reaction (Mo transfers electrons to the metallic ions of the salt converting them to metal (silver)). Figure 2 shows a Scanning Electron Microscopy (SEM) picture of the powder after printing; silver appears to coat the powder surface uniformly. At this stage, the printed part has no strength; the silver is porous and does not adhere to the powder.

To obtain strong bonding, the printed part was fired at 1000 °C for one hour under forming gas (silver melts at 960.8 °C) . Figure 3 shows an SEM picture of the powder after firing. Silver no longer covers the entire powder surface; it is randomly concentrated at various locations on the powder. Some of these locations are at the contact points of two adjacent powder particles and hold them together. The volume of the silver is calculated from the molarity of the solution and the volume fraction of the powder (about 60%) to be approximately 0.41% of the volume of the Mo powder. In this calculation it is assumed that the silver carbonate solution fills entirely the voids of the powder-bed. Silver carbonate, although less aggressive than silver nitrate, also causes irritation and silver staining of human skin and thus, continuous jet printing of silver carbonate is practical only as a research vehicle at this time.

2.2 Copper Nitrate on Mo Powder – Thermal Reduction

Noting that silver salts, in general, tend to cause skin irritation, attention was turned to copper salts. Copper nitrate solution was found not to cause skin burns or machine corrosion. The danger of inhalation posed by aerosol formation was mitigated by enclosing the 3D Printing machine and exhausting air from the enclosure through a ventilation system.

Droplets of a 0.43 molar water solution of copper nitrate ($Cu(NO_3)_2\ 2^1/_2H_2O$) were placed onto 66μm Mo powder and the powder was fired under forming gas for one hour at 1100 °C. The salt melts at about 114 °C and it reduces to the solid copper oxide (CuO). In the presence of hydrogen, CuO reduces to copper at about 240 °C. At 1083 °C the copper melts and binds the Mo powder. Assuming that the volume fraction of the powder is 60% and that the copper nitrate solution fully saturates the voids of the powder-bed, the volume of the copper is approximated as 0.20% of the volume of the Mo powder. Figure 4 shows an SEM picture of the resulting Cu necks that bind the 66μm Mo powder. The copper shows a clear tendency to concentrate in the "neck region" forming a well-defined neck. This tendency can be attributed to capillary forces which drive the salt to the necks while it dries and while it is melted.

However, parts made by the 3DP process with Mo powder can not be fired at a temperature high enough to melt copper due to the onset of sintering of the Mo powder. Firing the parts at a temperature close to the melting temperature of copper causes extensive sintering of the copper which holds the powder particles together. Although the strength of such a bonding was expected to be less than the one where the copper had melted it was not known if it was sufficient to result in parts with good handleable strength. This question was answered by firing printed parts at 1000 °C (Figure 5). These parts were intended for use as short run injection molding tools. The handling strength of the part was not satisfactory. A similar part, fired at 1030 °C, was equally weak (in this case removing the loose powder was problematic since the firing temperature was above the powder's T_S). Therefore, heat treating the copper necks below the melting point of copper is not an option if parts with good handle-able strength are to be produced.

The heat treatments described in the previous paragraph were done under a hydrogen atmosphere. Earlier attempts to fire the 2 in. x 3 in. x 7/8 in. part in a tube furnace under a forming gas atmosphere led to an incomplete reduction of the copper oxide. In particular, after

the forming gas heat treatment, the bottom-center portion of the part was black (the color of copper oxide). This incomplete reduction may be due to a slow diffusion rate of the hydrogen (of the forming gas) through the skeleton and/or due to a slow reduction rate.

2.3 Copper Nitrate and Silver Nitrate on Mo Powder – Forming an Alloy

To obtain necks that can be melted at temperatures less than the powder's T_S, printing a mixture of salt solutions from which a low melting temperature alloy can be derived, was considered. The following experiment demonstrates that strong bonding can be obtained by melting Ag-Cu alloy necks derived from a mixture of silver and copper nitrate salts.

The mixture used was a 2.21 molar $AgNO_3$ / 1.46 molar $Cu(NO_3)_2 \cdot 2^1/_2H_2O$ water solution (the solution was made by adding water to a mixture of 7.5g of $AgNO_3$ and 6.8g of $Cu(NO_3)_2 \cdot 2^1/_2H_2O$ to make a 20 ml solution). The copper to silver mass ratio in this solution is 0.39 which corresponds to the eutectic composition of the Ag-Cu system which has a melting temperature of 780 °C. Droplets of the solution were placed onto 31μm Mo powder and the powder was fired at 850 °C for one hour in a forming gas atmosphere. During this heat treatment the copper and silver salts reduced to their metals, which form an alloy. The Ag-Cu alloy melts and forms necks that bind the Mo powder. Figure 6 shows an SEM picture of the resulting Ag-Cu neck. Assuming that the volume fraction of the powder is 60% and that the salts solution fully saturates the voids of the powder-bed, the volume of the Ag-Cu alloy is calculated as 2.2% of the volume of the Mo powder.

This solution reduces the firing temperature to the point where the T_S requirement is satisfied even for the 31μm Mo powder. However, as noted previously, silver nitrate is extremely corrosive and hence, this material system is presented in this work as a point of reference for understanding and modeling shrinkage.

3 Shrinkage Measurements

Shrinkage usually occurs during drying of the binding solution and during firing. The former will be referred to as wet-dry shrinkage and the latter as dry-fired shrinkage. The shrinkage is measured by the following experimental technique.

3.1 Experimental Technique

A rectangular alumina tray is filled with powder and is struck 4-5 times in an attempt to obtain a packing density of the powder similar to that of the powder-bed in the printing machine (the piston that spreads the powder in the printing machine vibrates, while spreading, resulting in an increased packing density of the powder). Silicon carbide fibers (Textron Inc. of Lowell, MA) are then placed in the powder as shown in Figure 7. The fibers are approximately 5 mm long and

are placed approximately 25 mm apart; about 1 mm of the fibers extend above the powder. Using a pipette, the region between each pair of fibers is saturated with the binding solution [6].

The tray is then placed on a micrometer-driven x-y positioning stage with a resolution of 1μm, which is under an optical microscope. By moving the x-y stage and focusing on the fibers, the two perpendicular components (Δx and Δy) of the distance between the two fibers are measured and they are used to calculate the fiber-to-fiber distance. The diameter of the SiC fibers is 140μm and there is an inner carbon core of diameter 33μm within the fiber which is distinctly visible. The crosshairs of the optical microscope can be positioned at the center of this circle with repeatability of 5μm or less.

With the optical microscope and micrometer stage, each Δx and Δy measurement is reproducible to within 5 μm . In the worst case, this results in an error of approximately 10 μm in the fiber-to-fiber distance; therefore it results in an error of ± 20 μm in a shrinkage measurement (which consists of two distance measurements). For a 25 mm sample, this is an error of about ± 0.1%. As discussed below, the measurements were seen to be more reproducible than this rough estimation would indicate.

3.2 Results

Table 1a lists various shrinkage measurements. Data is presented for two powder materials, Mo and, for reference, alumina, a ceramic powder. In all cases, the powders are spherical and made by plasma melting. The alumina powder was chosen as a reference because it is available in spherical form in the proper size range, and because it is inert to water, a property that may not be shared by metals. Two sizes of Mo powder are used, a 66 μm average and a smaller powder, which ranges in size from 25-38 μm (denoted as 31 μm Mo powder). Shrinkage measurements were made with water alone, copper nitrate salt solution, silver carbonate salt solution, and copper-silver nitrate salt solution. Firing temperatures were chosen appropriate to the size of the Mo powder and the metal of the salt solution. As a result, not all combinations were tested. For example, only the copper silver salt solutions were tested for the smaller Mo powder because the lower sintering temperature of the small powder prevents its use with copper or silver alone. The multiple values for every powder-binder combination correspond to measurements from different samples. Table 1b lists the average and the sample standard deviation of the measurements shown in Table 1a.

As may be seen from these Tables, the results for the 66 μm powder support the hypothesis that adding metal by printing through the binder can lead to low shrinkage systems in 3D Printing. In particular, the wet-to-dry shrinkage for 66 μm Mo powder averages 0.03% over the two salts tested and this result may represent primarily measurement noise. Further, the dry-to-fired shrinkage averages 0.15% over the three salts tested. This result compares favorably with the 1.5% shrinkage typical in the standard process.

Nonetheless, the shrinkage for 66 μm Mo powder is clearly non-zero. Further, it is noted that the smaller Mo powder exhibits significantly higher shrinkages, both in the wet-to-dry

shrinkage and in the dry-to-fired shrinkage. With the goal of understanding this shrinkage behavior and, hopefully, of controlling it and further reducing its magnitude, a modeling effort was undertaken.

4 Modeling Of Shrinkage Caused By Liquid Necks

4.1 Mechanism Causing Shrinkage

Liquid necks impose attractive forces on neighboring powder particles and attempt to pull them closer together. On the other hand, the powder particles are not entirely free to move because they are mechanically constrained by their adjacent neighbors (Figure 8). Relative movement of the powder particles (and consequently shrinkage) occurs only when the attractive forces overcome the inter-particle friction of the powder. Therefore, shrinkage can be viewed as an equilibrium among the attractive forces between powder particles due to the liquid necks and the stiffness of the powder bed.

The shrinkage mechanism was investigated by independently studying the compressibility properties of the powder and the attractive forces induced by the liquid necks. This approach is analogous with the one used by Charnnarong [7] to study the shrinkage mechanism of alumina powder printed with colloidal silica. In that case, the attractive force was caused by the gelling and consolidation of the colloidal silica during drying and sintering.

In the following section, the attractive force, F, induced by the liquid necks is quantified. In section 4.3 we calculate an equivalent external isostatic pressure, $P_{eq.}$ which when applied to a collection of spherical particles results in inter-particle forces approximately equal to F. In section 4.4 we measure the compressibility of loose powder under external isostatic pressure. In section 4.5 the compressibility measurements are combined with the calculations of $P_{eq.}$ to predict the shrinkage that should be expected due to the presence of liquid necks.

4.2 Attractive Forces Between Spherical Powder Particles Induced by Liquids in the Necks

Figure 9, shows two spherical particles of radius R, held together by a liquid neck. The inter-particle force, F, due to capillary action of the liquid neck has two contributions, one due to the pressure difference caused by surface curvature and one due to the surface tension itself. As will be shown, the inter-particle force is relatively insensitive to the amount of liquid present, especially for small amounts of liquid. If the amount is increased from zero, the force due to the pressure difference starts out as attractive and decreases as more liquid is added, eventually becoming repulsive. At the same time, as liquid is increased from zero, the force due to surface tension starts out at zero and progressively increases, always being attractive between particles. Thus, as liquid is added to the necks, the two forces tend to compensate for one another, resulting in a force that is relatively constant with the amount of liquid.

Heady and Cahn [8] solved numerically the problem of capillary forces imposed on spherical particles by liquid necks, (they also solved the equivalent problem for the case of jagged particles

[9]). They used numerical means to solve for the shape of the liquid surface. Their results, are summarized in Figure 10. The attractive force is plotted as a function of the volume of the liquid neck, V, for different contact angles. The force, and the volume are non-dimensionalized by $R\sigma$ and R^3 respectively. F^* decreases monotonically with V^* from its maximum value at infinitesimal liquid volumes. F^* also decreases with increasing contact angle. For the case of $\theta = 0$, and small liquid volumes, the case of interest here, the attractive force can be approximated as:

$$F = 2\,\pi\,\sigma\,R. \tag{4.1}$$

4.3 Calculation of Equivalent Pressure

An estimate needs to be found of the equivalent external pressure, $P_{eq.}$, that when applied isostatically to a balloon filled with spherical particles of radius, R, will result in an inter-particle force, F. Such an estimate can be obtained by making a simplified assumption on the way spheres arrange themselves when they are poured into a balloon. For the purposes of this calculation, it is important that the assumed arrangement will correspond to a coordination number (the number of other particles in contact with a given particle) and a packing fraction close to that obtained when uniform size spheres are poured into a balloon. It was found [10] that lead shot with a particle size of 3.78 mm poured into a glass beaker have a packing fraction equal to 55.3% and a coordination number equal to 6.92. A simple-cubic arrangement has a packing fraction of 52% and coordination number of six. It is therefore expected to give a reasonable estimate of $P_{eq.}$. By dividing the sum of the forces acting on a side (the (100) crystallographic plane) of the cubic cell (F) by the area of the side of the cube ($4R^2$), $P_{eq.}$ is calculated as:

$$P_{eq.} = F/(4R^2) \tag{4.2}$$

The same value is obtained by summing the forces acting on the diagonal plane of the cubic cell (the (110) crystallographic plane) and dividing by the corresponding area.

Therefore, by substituting equation (4.1) into equation (4.2) we find,

$$P_{eq.} = \pi\,\sigma/(2R) \tag{4.3}$$

Table 2 shows the values of $P_{eq.}$ for different powders and liquid necks as calculated from equation (4.7). The following values for surface tension were used: σ_{water} = 0.073 N/m, σ_{Ag} = 0.893 N/m, σ_{Cu} = 1.301 N/m, and $\sigma_{Ag\text{-}Cu\,[71.9:28.1]}$ = 1.008 N/m. The surface tension of the Ag-Cu alloy can be calculated [12] from the values of the surface tension of the silver and the copper by means of an additive rule (mass fraction of Ag x σ_{Ag} + mass fraction of Cu x σ_{Cu}).

4.4 Compressibility of Loose Powder

4.4.1 Response of Loose Powder to an External Isostatic Pressure

There are two mechanisms involved in the isostatic deformation of loose powder; (i) rearrangement-restacking of the particles, and ii) elastic-plastic deformation. Particle rearrangement and restacking takes place at low pressure as particles slide relative to one another and reorder into a tighter formation [7]. The elastic-plastic deformation mechanism is not relevant to this study because it occurs at pressures above those listed in Table 2. The rearrangement and restacking response of loose powder to an external pressure is expected to depend on the powder's shape, size, size distribution, surface characteristics and initial packing fraction. The complexity of the problem makes it intractable to any analytical investigation and points to an experimental study.

4.4.2 Experimental Set-Up

The compressibility of loose powder is measured by placing the powder in a balloon, applying an external isostatic pressure to it and measuring its change of volume. Figure 11 shows a sketch of the experimental set-up. The external isostatic pressure is created by generating a vacuum inside the balloon. A tube is attached to a balloon. The tube has a filter at its end, which prevents the passage of water and powder but allows the passage of air. The balloon is submerged in water; the volume change of the balloon is determined by recording the surface level of the water.

The linear shrinkage, S_L, is calculated from the measured volumetric shrinkage, $S_V=\Delta V_P/ V_o$, according to the relationship:

$$S_L = 1-(1-S_V)^{1/3}.$$

The maximum pressure (1 atm.) that can be obtained with this experimental set-up is sufficient for the needs of this study (see Table 2).

4.4.3 Measurements

Figure 12, shows the percentage linear shrinkage of 31 μm and 66 μm Mo powders as a function of pressure for different initial packing fractions. The finer powder is more compressible than the larger one. It can be seen that the compressibility of the powder depends strongly on the initial packing fraction. Powder which starts with a higher initial packing density is stiffer. A higher initial packing fraction indicates a more stable particle arrangement and consequently higher resistance to rearrangement. The initial packing fraction of the 31 μm Mo powder tends to be less than that of the 66 μm powder. This behavior can be attributed to the larger surface area of the smaller powder which results in higher inter-particle adhesion and friction and consequently to higher resistance to tighter packing.

The initial packing fractions obtained with this experimental set-up are close to that obtained by pouring the powder in a graduated cylinder and striking the cylinder a few times. For instance, 66 μm Mo powder was poured into a graduate cylinder and its packing fraction was measured as 57.1%. After the cylinder was manually struck 4-5 times, its packing fraction was measured as 60.2% (the powder was then tapped causing an increase in its packing fraction to 63%). Therefore, it is expected that the packing fractions involved in the compressibility measurements are comparable to those involved in the shrinkage measurements of section 3 (the powder was struck before taking the shrinkage measurements).

4.5 Combination

The compressibility measurements, combined with the analysis of section 5.2 and 5.3 can be used to predict the shrinkage caused by liquid necks. Figure 13 shows the compressibility measurements of the 66 μm Mo powder for three different initial packing fractions.

Four vertical lines are drawn to identify the $P_{eq.}$ that correspond to water (1.7 KPa), silver (21.2 KPa), silver/copper eutectic alloy (24.0 KPa) and copper (30.9 KPa) necks; these values are taken from Table 2. The intersections of these lines with those of the compressibility measurements can be used to predict the shrinkage caused by the related liquid necks. The $P_{eq.}$ = 1.7 KPa line predicts that the shrinkage caused by water necks, will be less than 0.05% for all three initial packing fractions. For comparison, the wet-dry shrinkage measurements of the water-printed 66 μm Mo powder (taken from Table 1a) are superimposed on the figure as the marks on this vertical line. The $P_{eq.}$ = 30.9 KPa line predicts that the shrinkage caused by liquid copper necks will range from 0.12% to 0.17% depending on the initial packing fraction. The marks on this line represent the dry-fired (1100 °C) shrinkage of the copper nitrate printed 66 μm Mo powder and they illustrate the proximity between predicted and measured shrinkage. The same consistency is found for the cases of silver and silver/copper necks.

Figure 14 shows the compressibility measurements of the 31 μm powder. The two vertical lines identify the $P_{eq.}$ that correspond to water (3.7 KPa) and silver/copper (51.1 KPa) necks. The marks on these lines, which identify the measured shrinkage (see Table 1a) caused by water and silver/copper nitrates, are close to the predicted values of shrinkage.

A note should be made on the effect of the liquid salts on shrinkage. Although the surface tension of the melted salts under consideration are not known, they are expected to be close to that of water [12]. Therefore they are expected to cause shrinkage similar to that of water during drying. This expectation was verified by measuring the dry-fired (300 °C) shrinkage of the copper nitrate printed 66μm Mo powder and the dry-fired (490 °C) shrinkage of the copper/silver nitrate printed 31μm Mo powder (Table 1a). These heat treatments were carried out at temperatures higher than the melting point of the salts.

The larger shrinkage of the 31μm Mo powder, compared to that of 66μm Mo powder, caused by water and silver/copper necks, can be explained by the fact that the former powder is

more compressible than the latter (Figure 12) in combination with the fact that the $P_{eq.}$ is inversely proportional to the size of the powder. Finally, it should be noted that the wet-dry water shrinkage of the 31μm Mo powder is larger than that of the 30μm alumina powder (see Table 1); this deviation can be explained by a possible reaction between the water and the Mo powder.

5 Conclusion

Salt solutions can be used by 3D Printing to produce metal skeletons. With the appropriate heat treatment, the metal of the salt can form metallic necks that bind the powder particles; melting the metal (or alloy) of the salts is critical to obtain strong skeletons. The average shrinkage caused by silver, copper and silver-copper necks on the 66 μm Mo powder is ~0.15% and the shrinkage caused by the silver-copper necks on the 31 μm Mo powder is 0.35%. These shrinkages compare favorably with the 1.5% shrinkage obtained by the standard sinter-based method. To fully evaluate the potentials of these systems in improving the dimensional control of the printed parts, the uncertainty associated with these shrinkages should be determined.

Issues concerning operator safety and damage to the machine, restrict the type of salt solutions that may be used in a given type of ink-jet printhead. Improved automation of the printing machine combined with the use of corrosion resistant materials are expected to mitigate the effect this restriction. However, even the highly corrosive silver salts can be used in Three Dimensional Printing when dispensed by a drop-on-demand printhead, where the volume of material dispensed is small and easily controlled. Despite its health hazards, the copper nitrate solution may be practically applied to 3DP with minor modifications on the printing machine. This solution was printed into a Mo/Ag powder bed and injection molding tools were fabricated which suggest that this material system can potentially be used to fabricate parts with good surface finish and good handle-able strength.

It was hypothesized that the capillary forces induced by the liquid necks was causing a shrinkage of the metal skeleton. By studying independently the compressibility of the powder and the capillary forces, sufficient support for this hypothesis was found. The compressibility of the powder was determined by applying an external isostatic pressure on a balloon filled with loose powder and measuring its change of volume. The force between spherical powder particles induced by liquid necks was determined analytically assuming a circular profile for the liquid meniscus.

This study also explains the difference in the shrinkage between the 31 μm and 66 μm Mo powder. The compressibility measurements indicate that the shrinkage caused by liquid necks can be drastically reduced by increasing the packing fraction of the spread powder.

References

[1] Sachs, E. Haggerty, J., Williams, P., and Cima, M., *U.S. Patent*, 5204055, 1993.

[2] Sachs, E, Cima, M., Williams, P., Brancazio, D., and Cornie, J., "Three Dimensional Printing: Rapid Tooling and Prototypes Directly From a CAD Model", Journal of Engineering for Industry, Vol 114, No. 4, November 1992, p. 481-488.
[3] Sachs, E., Cima, M., Bredt, J., Curodeau, A. "CAD-Casting: The Direct Fabrication of Ceramic Shells and Cores by Three Dimensional Printing", Manufacturing Review, Vol 5, No 2, June 1992, p. 118-126.
[4] Sachs, E., et al. "Injection Molding Tooling by Three Dimensional Printing.", Rapid Prototyping and Manufacturing '96, Dearborn MI, Rapid Protyping Association of SME, 1996.
[5] Sachs, E., Hadjiloucas, C., Allen, S., Yoo, H., "Metal and Ceramic Containing Parts Produced From Powder Using Binders Derived From Salt," Patent Pending.
[6] Yoo, H., "Reactive Binders for Metal Parts Produced by Three Dimensional Printing," M.S. Thesis, Massachusetts Institute of Technology, Cambridge, 1997.
[7] Charnnarong, J., "The Drying Shrinkage in Three Dimensional Printing and its Dependence on the Properties of the Powder and the Binder," Ph.D. Thesis, Massachusetts Institute of Technology, Cambridge 1996.
[8] Heady, R. B., Cahn, J. W., "Analysis of the Capillary Forces in Liquid-Phase Sintering of Spherical Particles," Journal of the American Ceramic Society, vol. 1, January 1970 [7], p. 185-189.
[9] Cahn, J. W., Heady, R. B., "Analysis of the Capillary Forces in Liquid-Phase Sintering of Jagged Particles," Journal of the American Ceramic Society, vol. 53, January 1970 [7], p. 406-409.
[10] ASM Handbook, Vol. 7. Powder Metallurgy, p. 296.
[11] R. K. McGeary "Mechanical Packing of Spherical Particles," Journal of the American Ceramic Society, vol. 44, 1961, p.513.
[12] "Surface Chemistry" Bikerman, Second Edition.

Tables and Figures

	Water	$Cu(NO_3)_2$	Ag_2CO_3	Cu/Ag Nitrates
31 μm Mo				
wet-dry:	0.08; 0.08; 0.11			0.04; 0.08; 0.05
dry-490 °C				0.03; 0.05
dry-850 °C				0.36; 0.35; 0.35
66 μm Mo				
wet-dry:	0.01; 0.02; 0.02	0.01; 0.04; 0.02; 0.05	0.00; 0.06; 0.02	
dry-300 °C		0.02; 0.01; 0.03		
dry-1000 °C			0.13; 0.15; 0.11	0.12; 0.17; 0.14
dry-1100 °C		0.17; 0.17; 0.18		
30 μm Alumina				
wet-dry:	0.02; 0.02; 0.03			

Table 1a Percentage Linear Shrinkage: Wet-dry is the shrinkage due to drying and dry-fired is the shrinkage due to firing. The multiple values for each powder-binder combination correspond to different measurements

	Water	$Cu(NO_3)_2$	Ag_2CO_3	Cu/Ag Nitrates
31 μm Mo				
wet-dry:	0.09±0.02			0.06±0.02
dry-490 °C				0.04±0.01
dry-850 °C				0.35±0.01
66 μm Mo				
wet-dry:	0.02±0.01	0.03±0.02	0.03±0.03	
dry-300 °C		0.02±0.01		
dry-1000 °C			0.13±0.02	0.14±0.03
dry-1100 °C		0.17±0.01		
30 μm Alumina				
wet-dry:	0.02±0.01			

Table 1b The results of Table 1a are presented here as: average ± sample standard deviation

	Equivalent Pressure [KPa]			
	Water	Ag	Cu	Ag/Cu
31 μm Mo	3.7			51.1
66 μm Mo	1.7	21.2	30.9	24.0
30 μm Alumina	3.8			

Table 2 Equivalent Pressure

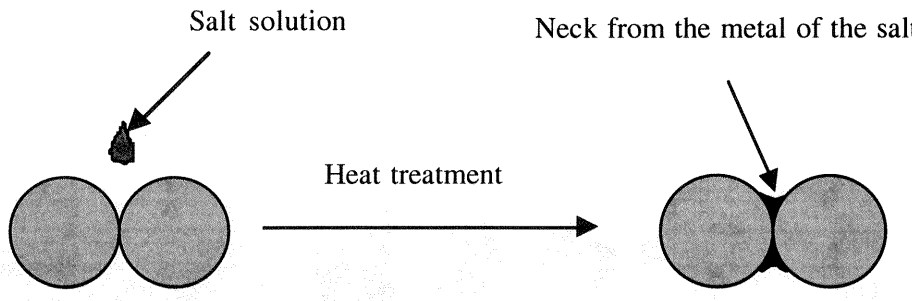

Figure 1 Principle of the Salt Binding Method

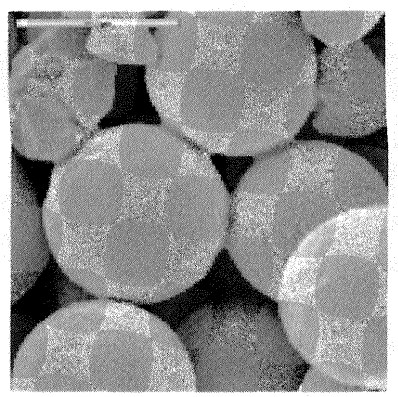

Figure 2 Mo Powder Printed with Silver Carbonate

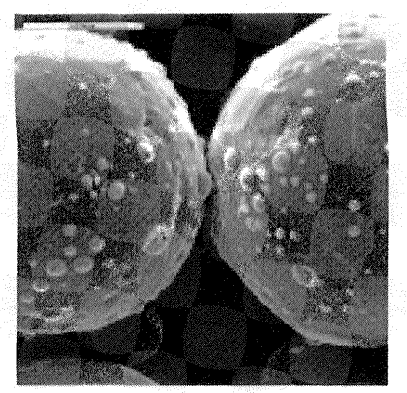

Figure 3 Mo Powder Printed with Silver Carbonate and Fired at 1000°C

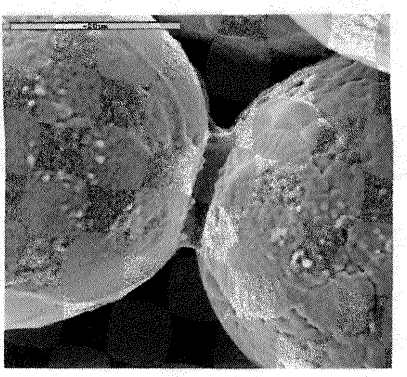

Figure 4 66 μm Mo Powder Printed with Copper Nitrate and Fired at 1100 °C

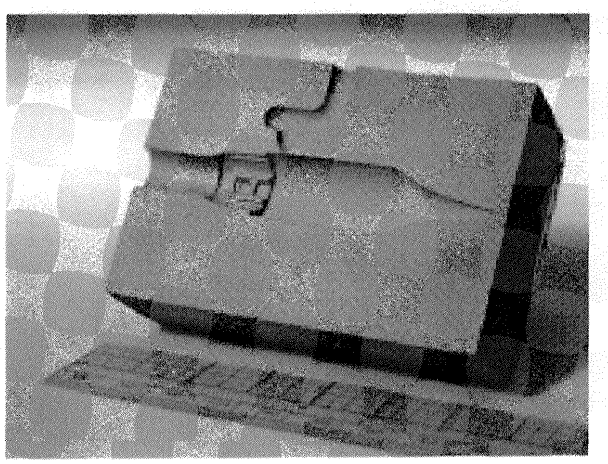

Figure 5 Mo-Cu Injection Molding Tool

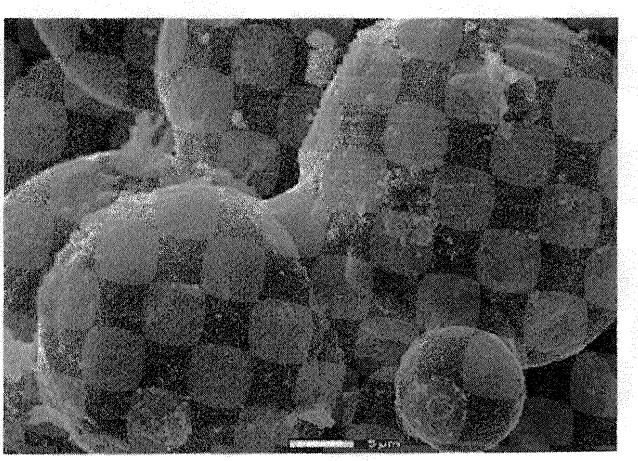

Figure 6 31μm Mo Powder Printed with Silver Nitrate and Copper Nitrate and Fired at 850°C

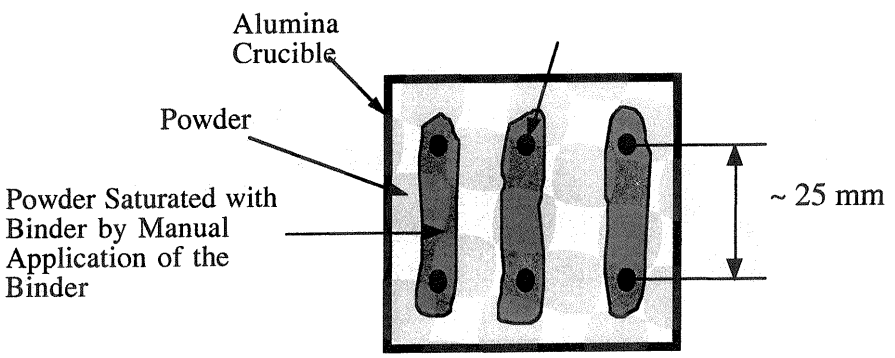

Figure 7 Shrinkage Test Set-Up

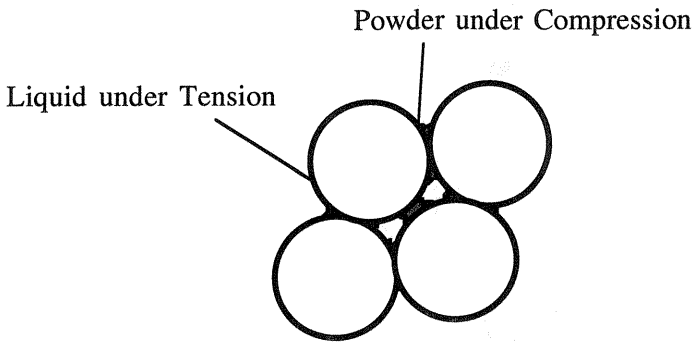

Figure 8 Liquid Necks Attempt to Pull Neighboring Particles Closer Together; Contiguous Particles Resist this Motion.

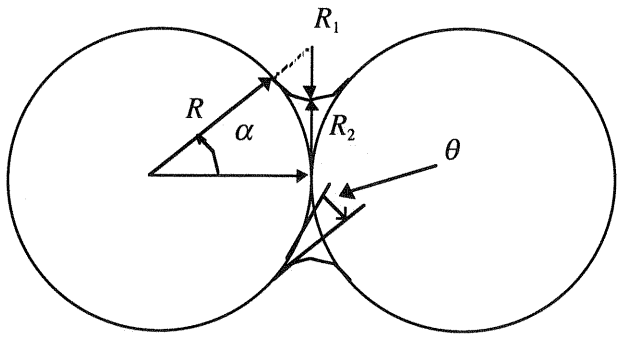

Figure 9 Liquid Neck between Spherical Particles

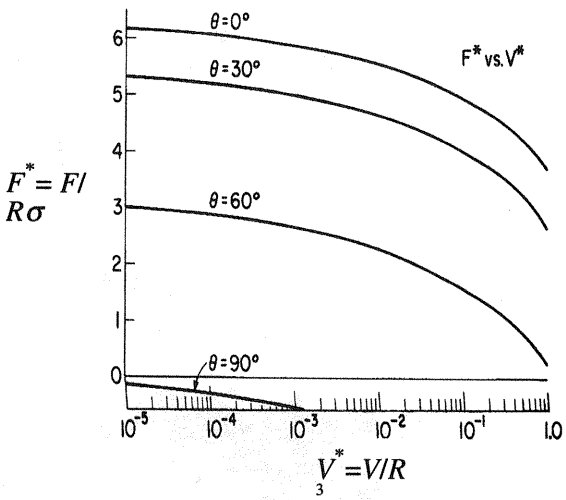

Figure 10 Interparticle Force as a Function of the Volume of the Liquid Neck; Taken from Heady and Cahn Study [8]

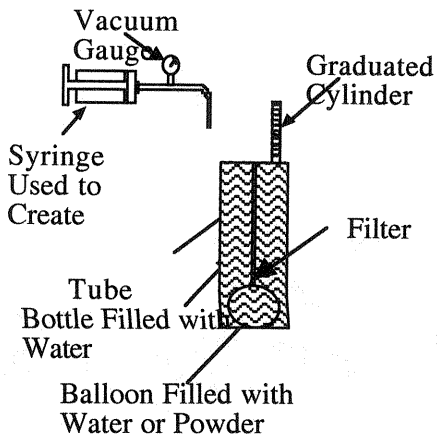

Figure 11 Experimental Set-up Used to Measure the Compressibility of Loose Powder

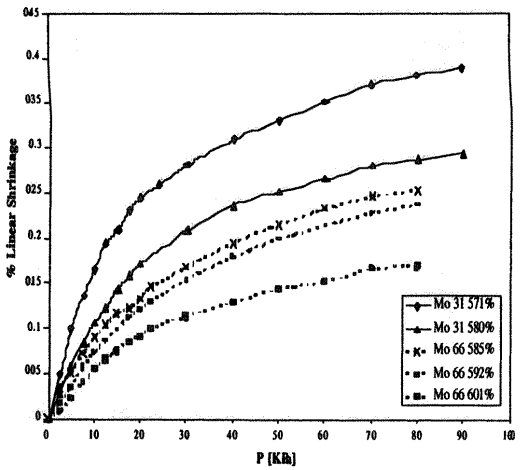

Figure 12 Compressibility Measurements of the 31μm and 66 μm Mo Powder

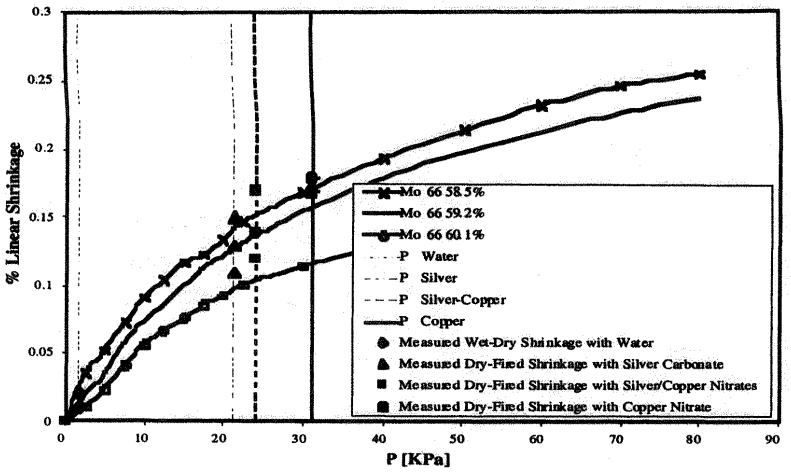

Figure 13 Predicted and Measured Shrinkage of the 66μm Mo Powder

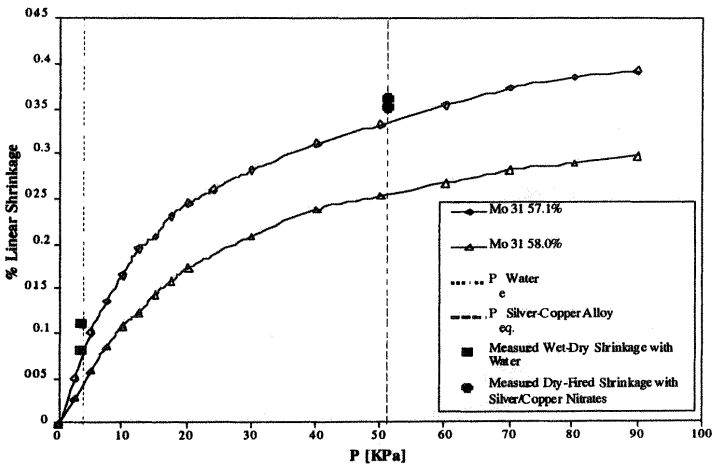

Figure 14 Predicted and Measured Shrinkage of the 31μm Mo Powder